LETTER

doi:10.1038/nature11267

The dynamic disulphide relay of quiescin sulphydryl oxidase

Assaf Alon[1], Iris Grossman[1], Yair Gat[1], Vamsi K. Kodali[2], Frank DiMaio[3], Tevie Mehlman[4], Gilad Haran[5], David Baker[3], Colin Thorpe[2] & Deborah Fass[1]

Protein stability, assembly, localization and regulation often depend on the formation of disulphide crosslinks between cysteine side chains. Enzymes known as sulphydryl oxidases catalyse *de novo* disulphide formation and initiate intra- and intermolecular dithiol/disulphide relays to deliver the disulphides to substrate proteins[1,2]. Quiescin sulphydryl oxidase (QSOX) is a unique, multi-domain disulphide catalyst that is localized primarily to the Golgi apparatus and secreted fluids[3] and has attracted attention owing to its overproduction in tumours[4,5]. In addition to its physiological importance, QSOX is a mechanistically intriguing enzyme, encompassing functions typically carried out by a series of proteins in other disulphide-formation pathways. How disulphides are relayed through the multiple redox-active sites of QSOX and whether there is a functional benefit to concatenating these sites on a single polypeptide are open questions. Here we present the first crystal structure of an intact QSOX enzyme, derived from a trypanosome parasite. Notably, sequential sites in the disulphide relay were found more than 40 Å apart in this structure, too far for direct disulphide transfer. To resolve this puzzle, we trapped and crystallized an intermediate in the disulphide hand-off, which showed a 165° domain rotation relative to the original structure, bringing the two active sites within disulphide-bonding distance. The comparable structure of a mammalian QSOX enzyme, also presented here, shows further biochemical features that facilitate disulphide transfer in metazoan orthologues. Finally, we quantified the contribution of concatenation to QSOX activity, providing general lessons for the understanding of multi-domain enzymes and the design of new catalytic relays.

The introduction of disulphide bonds into folding proteins is typically accomplished by enzyme pairs[1,2]; one enzyme generates disulphides *de novo*, often with the aid of a bound cofactor, and the second enzyme acquires these disulphides by dithiol/disulphide exchange and passes them on to substrate proteins. Examples of such partnerships include DsbB and DsbA in the *Escherichia coli* periplasm and, in eukaryotes, Ero1 and protein disulphide isomerase (PDI) in the endoplasmic reticulum and Erv1 and Mia40 in the mitochondrial intermembrane space. A partnership between vitamin K epoxide reductase (VKOR) and membrane-anchored PDI-family proteins has also been identified in the endoplasmic reticulum[6]. The QSOX enzymes[3] are the only known example of conserved concatenation of disulphide-generating and disulphide-transferring modules within a single polypeptide (Fig. 1a), although a VKOR-like protein is fused to its partner in a few species[7]. Domain fusion may allow QSOX to function under dilute conditions in extracellular environments[8–10]; other disulphide-generating enzymes function in sequestered intracellular compartments with high local concentrations of disulphide-transferring enzymes.

Formation and transfer of disulphide bonds in QSOX are mediated by redox-active cysteine pairs in the canonical pattern Cys-X-X-Cys (Fig. 1a). One such dicysteine motif is in a thioredoxin-fold domain (Trx1) related to the redox-active domains of PDI. Another is in a flavin adenine dinucleotide (FAD)-binding domain (Erv) related to the mitochondrial enzyme Erv1. The proposed QSOX mechanism[11,12] involves the generation of disulphides catalytically at the FAD-proximal dicysteine motif, intramolecular disulphide transfer to the Trx1 domain and finally intermolecular dithiol/disulphide exchange with the substrate (Fig. 1a). How the Trx1 redox-active residues interact alternately with the Erv domain and with substrate proteins remains unclear.

The *Trypanosoma brucei* parasite, the cause of African trypanosomiases, encodes a QSOX enzyme (TbQSOX)[13]. We determined the X-ray crystal structure of TbQSOX to 2.3 Å resolution (Supplementary Table 1). In the crystallized configuration, the Trx1 redox-active site faces outwards (Fig. 1b), where it would be readily accessible to nucleophilic attack by substrate cysteine thiolates. However, in this position, the Trx1 active site is 42 Å away from the Erv active site and would thus be unable, after disengaging from the substrate, to accomplish the next step in the proposed relay mechanism (Fig. 1a).

To test whether the distance between redox-active sites in the TbQSOX crystal structure is representative of their average separation in solution, we used fluorescence resonance energy transfer (FRET) spectroscopy. TbQSOX Cys 72 was mutated to leave one cysteine (Cys 69) free within the Trx1 active site for labelling with the donor fluorophore Pacific Blue C_5-maleimide. The bound FAD, although not fluorescent, served as an energy acceptor at the Erv active site, and the decrease in donor fluorescence was taken to reflect FRET efficiency. The use of an intrinsic chromophore as one member of the FRET pair minimized potential perturbations due to labelling. An average distance of 55 Å was measured between the label at position 69 and FAD (Supplementary Table 2), supporting a requirement for major conformational changes during the QSOX disulphide relay. Donor labels introduced at a variety of other positions across the enzyme surface provided a set of ensemble-averaged distances characterizing the resting state of the enzyme (Fig. 1c, Supplementary Figs 1–3 and Supplementary Tables II and IIIa–c).

To obtain structural insight into the intramolecular disulphide-transfer step (see Supplementary Discussion), we eliminated the second cysteine of both TbQSOX redox-active Cys-X-X-Cys motifs. The resulting mutant is able to form, but not resolve, the interdomain disulphide essential for catalysis. We purified (Supplementary Fig. 4) and crystallized the closed, interdomain disulphide-bonded version of TbQSOX ($TbQSOX_C$) and solved its structure to 3.3 Å resolution. When compared with the wild-type enzyme, a ~165° rotation of the Trx1 domain and associated helix brings the two redox-active sites within covalent-bonding distance in $TbQSOX_C$ (Fig. 1d and Supplementary Movie 1). Consistent with this closed configuration being a transient state during enzyme turnover, the surface complementarity between the $TbQSOX_C$ redox-active domains is greater than

[1]Department of Structural Biology, Weizmann Institute of Science, Rehovot 76100, Israel. [2]Department of Chemistry and Biochemistry, University of Delaware, Newark, Delaware 19716, USA. [3]Department of Biochemistry, University of Washington, Seattle, Washington 98195, USA. [4]Department of Biological Research Support, Weizmann Institute of Science, Rehovot 76100, Israel. [5]Department of Chemical Physics, Weizmann Institute of Science, Rehovot 76100, Israel.

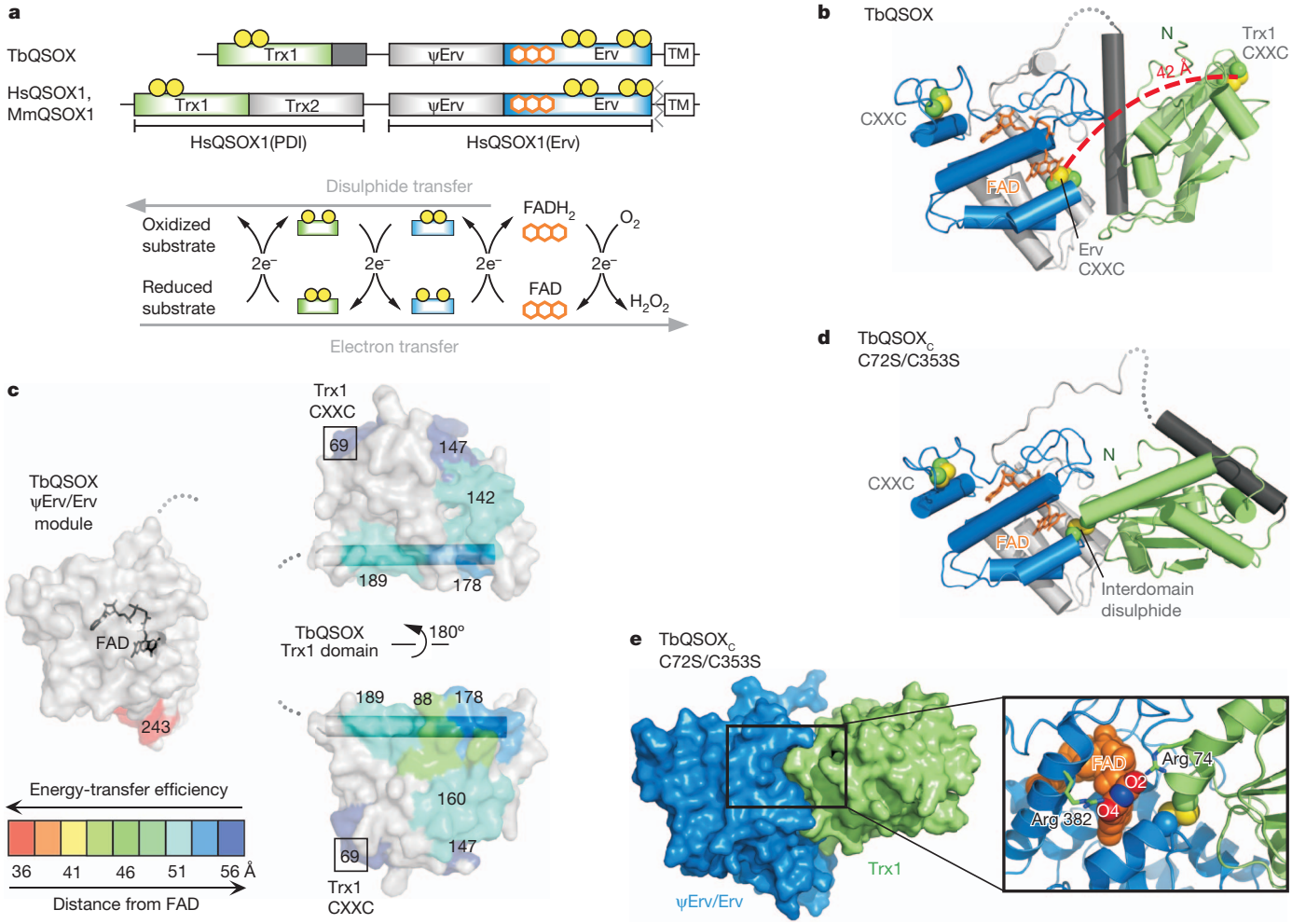

Figure 1 | TbQSOX undergoes domain reorientation to accomplish disulphide relay. **a**, Cys-X-X-Cys motifs are illustrated as pairs of yellow balls in maps of trypanosome and mammalian QSOX enzymes. Other cysteines are shown in Supplementary Fig. 13. Fused hexagons represent the FAD cofactor. A degenerate Erv-like domain[17] is designated 'ψErv'. Arrows depict the electron-transfer relay from reduced substrates to molecular oxygen and the corresponding outward flow of disulphide equivalents from QSOX to its substrates. TM, transmembrane. **b**, TbQSOX structure coloured according to **a**. Disulphides in Cys-X-X-Cys motifs are in space-filling representation (Cβ atom, green; sulphur, yellow). Structure stereo views are depicted in Supplementary Fig. 14. **c**, Colour-coded intramolecular distances between fluorophore-labelled TbQSOX cysteines and the bound FAD cofactor. **d**, Structure of $TbQSOX_C$. **e**, Surface representation of $TbQSOX_C$ and zoom into the interdomain interface. FAD is in space-filling representation, and oxygen atoms in the isoalloxazine ring are coloured red and labelled. Structure figures were made using PyMOL (http://www.pymol.org).

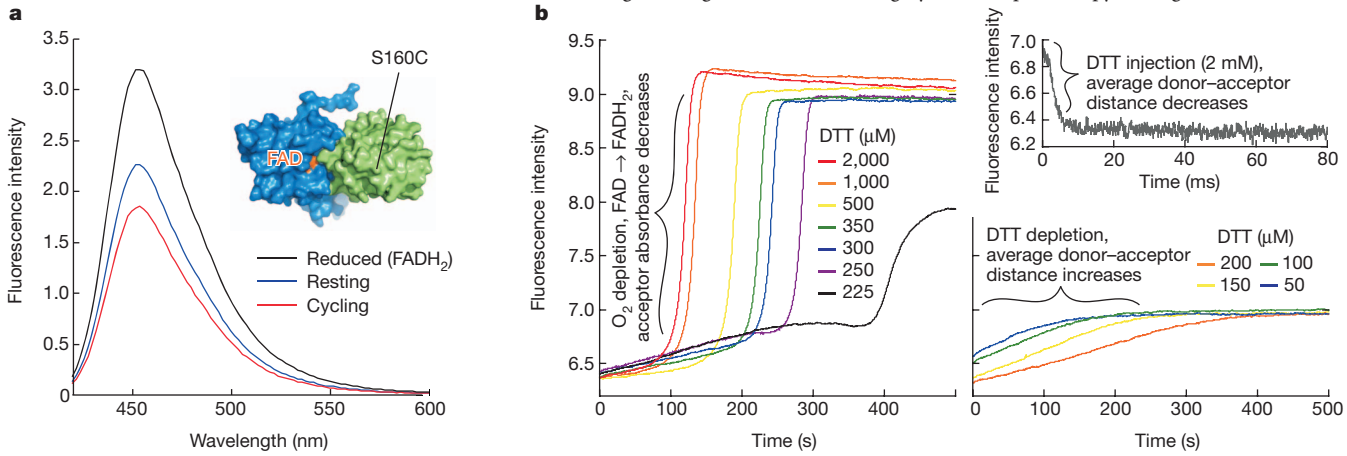

Figure 2 | Changes in the TbQSOX conformational ensemble during catalysis. **a**, Fluorescence of Pacific Blue conjugated at position 160 in resting TbQSOX (blue), TbQSOX oxidizing the model substrate dithiothreitol (DTT; red) and after oxygen depletion and conversion of the energy acceptor FAD to $FADH_2$ (black). Inset, surface representation of $TbQSOX_C$, as in Fig. 1e, with FAD and donor-labelling site indicated. **b**, Kinetics of donor fluorescence during TbQSOX oxidation of DTT. On DTT injection, labelled enzyme rapidly converts to a state showing greater FRET efficiency (top right panel). Other panels show longer timescales at various initial DTT concentrations. At starting DTT concentrations above ~200 μM (left panel), oxygen becomes limiting, the flavin becomes trapped as $FADH_2$ (see Fig. 1a), flavin absorbance at ~450 nm drops markedly and donor fluorescence increases correspondingly. At starting DTT concentrations of 200 μM or below (bottom right panel), DTT is limiting and the enzyme returns to its oxidized, resting state.

non-evolved interfaces (represented by crystal contacts) and less than stable protein–protein interactions[14].

In addition to illustrating the functionally important reorientation of the redox-active sites, the $TbQSOX_C$ structure shows how closure of the Trx1 domain over the FAD-binding site may enhance the active-site chemistry for disulphide formation. In the reduced, anionic form of flavin, negative charge is distributed over atoms N1, O2 and O4 of the isoalloxazine ring. Other disulphide-forming enzymes position a basic residue near the cofactor to stabilize this negative charge[15,16]. In $TbQSOX_C$, the Trx1 domain contributes an arginine side chain (Arg 74) as an interaction partner for the FAD O2 atom (Fig. 1e), which may promote formation of a thiol–flavin charge-transfer complex and, in turn, a reduced state of FAD. Indeed, the TbQSOX Arg74Ala mutant is substantially less active than wild type (Supplementary Fig. 5). Other basic residues within the Erv domain (that is, His 356 and Arg 382) may further modulate the electrostatic environment of the FAD.

A second FRET study was conducted, this time monitoring energy transfer kinetically in the presence of substrate. The TbQSOX mutant with a donor fluorophore at residue 160 (Supplementary Table IIIc) showed a reproducible FRET increase when substrate was added (Fig. 2a). As expected, when oxygen was not limiting, the FRET signal returned to resting values as the substrate was exhausted (Fig. 2b). These observations indicate that the labelled position is closer to FAD in cycling TbQSOX than in the resting, native ensemble, further supporting conformational changes during catalysis.

Although TbQSOX has conserved functional features characteristic of the QSOX family, it is one of the most divergent orthologues. TbQSOX lacks a domain (Trx2) found in metazoan QSOX enzymes (Fig. 1a), and its Trx1 redox-active motif, Cys-Gly-Ala-Cys, differs from the Cys-Gly-His-Cys common to other QSOX proteins and to PDI-family proteins. We therefore expanded our study to include the architecture and dynamics of mammalian QSOX enzymes.

The structure of *Homo sapiens* QSOX1 (HsQSOX1) was solved in two complementary fragments, HsQSOX1(PDI) and HsQSOX1(Erv)[17] (Fig. 1a), crystallized separately (Fig. 3a and Supplementary Fig. 6). The HsQSOX1 domains containing redox-active Cys-X-X-Cys motifs were found to be similar to their TbQSOX counterparts (Supplementary

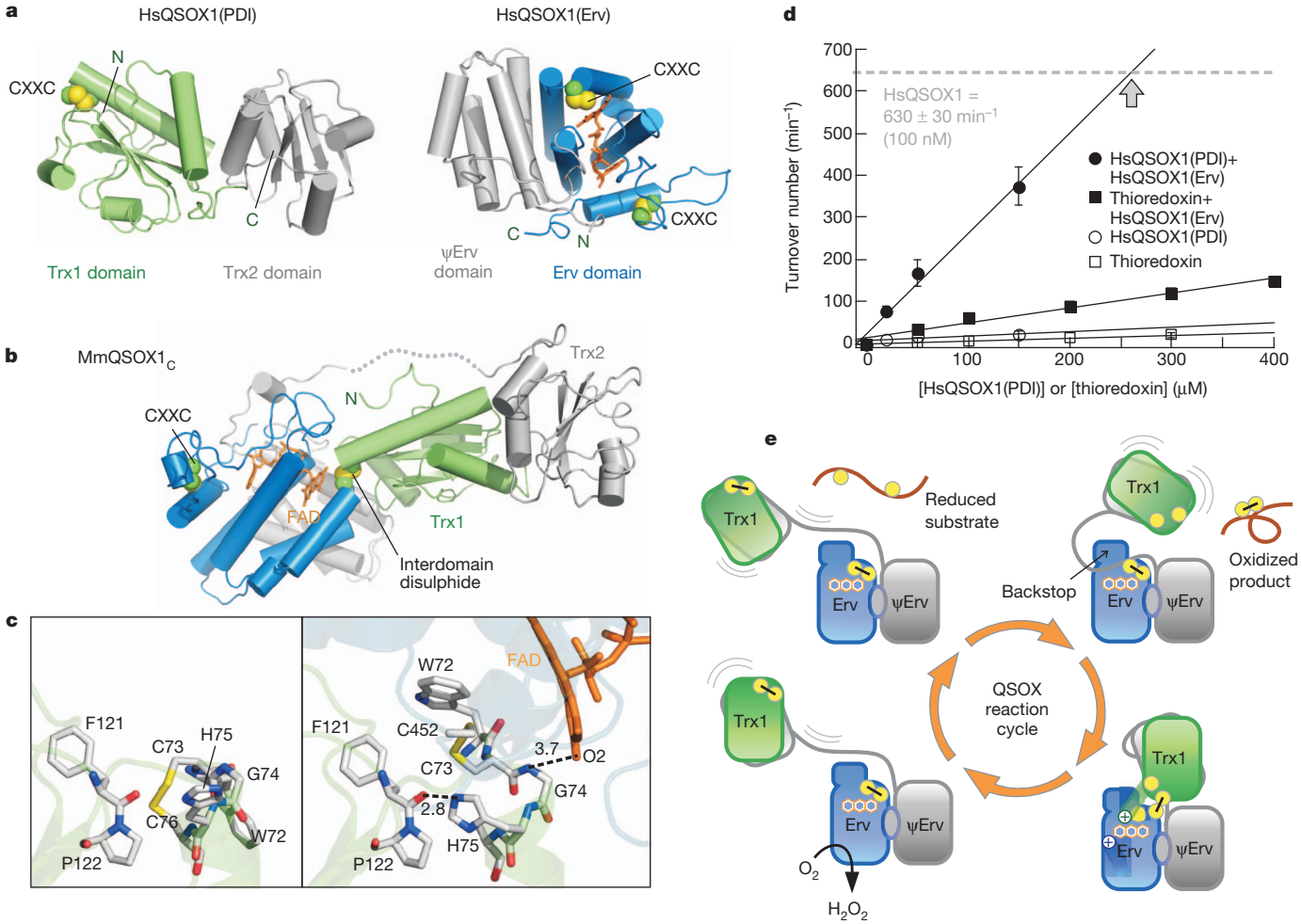

Figure 3 | Mammalian QSOX and mechanistic insights into the QSOX catalytic cycle. **a**, The structures of HsQSOX1(PDI) and HsQSOX1(Erv). Disulphides in Cys-X-X-Cys motifs are shown. Other cysteines appear in Supplementary Fig. 13. **b**, Structure of $MmQSOX1_C$. **c**, A comparison of HsQSOX1(PDI) (left) with $MmQSOX1_C$ (right) shows rearrangements in the Trx1 redox-active region on formation of the disulphide-transfer intermediate. Interatomic distances (dashed lines) are in Ångstrom. Residue numbering is according to MmQSOX1. **d**, Tethering increases the effective concentration of the HsQSOX1 disulphide-transferring module. Initial oxygen consumption rates were recorded for 100 nM HsQSOX1(Erv) and varying concentrations of HsQSOX1(PDI) (filled circles) or thioredoxin (filled squares) after injection of DTT. Grey dashed line indicates the turnover number for intact HsQSOX1, measured at 100 nM. By extrapolation, ~250 μM HsQSOX1(PDI) with 100 nM HsQSOX1(Erv) would be expected to support a similar reaction rate (grey arrow). Error bars, s.d. **e**, Summary of the structural basis of the QSOX catalytic mechanism, as shown in this study. Adjacent yellow balls with black bar indicate disulphide bonds; separated yellow balls indicate reduced thiols or thiolates. The '+' symbols in the closed conformation (bottom right) represent arginine side chains from either the Trx1 domain (in TbQSOX) or the Erv domain (in TbQSOX and mammalian QSOX1) that may contribute to the electron-withdrawing ability of the FAD. The 'backstop' represents conserved Erv domain loops (Supplementary Fig. 9).

Table 4). Outside of these regions, the human and parasite structures are more divergent. In particular, HsQSOX1 has the Trx2 domain but lacks the long helix of TbQSOX (Fig. 1b). The two functional modules of HsQSOX1 seem to be tethered flexibly to one another, as found for TbQSOX (Supplementary Fig. 7 and Supplementary Table 5).

Mammalian QSOX mutants designed to mimic the interdomain disulphide-transfer intermediate, analogous to $TbQSOX_C$, were constructed. The *Mus musculus* structure, $MmQSOX1_C$, solved to 2.4 Å resolution, demonstrated how disulphide transfer readily accommodates the extra domain in metazoan QSOX (Fig. 3b). Moreover, some features that may orient the two enzyme halves are conserved (Supplementary Figs 8 and 9). One difference between $TbQSOX_C$ and $MmQSOX1_C$, however, is the presence of the histidine residue (His 75) in the MmQSOX1 Trx1 Cys-Gly-His-Cys motif. His 75 appeared in two distinct rotamers in the $MmQSOX1_C$ crystals, providing insight into the dynamics of catalysis (Supplementary Figs 10 and 11). In one configuration, His 75 would be in a position to interact transiently with the thiolate of the Erv active-site cysteine Cys 452 during resolution of the interdomain disulphide intermediate (Supplementary Fig. 11). A comparison of HsQSOX1(PDI) and $MmQSOX1_C$ shows how the end of the Trx1 redox-active helix rearranges on interaction with the FAD-binding domain (Fig. 3c). No Trx1 side chain comparable to TbQSOX Arg 74 interacts with the flavin in $MmQSOX1_C$, but unpaired -NH groups at the amino terminus of the $MmQSOX1_C$ Trx1 redox-active helix approach the FAD O2 atom (Fig. 3c). Furthermore, Arg 490 is recruited from within the Erv domain for interaction with FAD O4 (Supplementary Fig. 11), like its corresponding residue in TbQSOX (Arg 382). In summary, many structural and dynamic properties of mammalian and trypanosome QSOX proteins are similar, and both enzymes seem to recruit electron-withdrawing groups to modulate active-site electrostatics during catalysis. However, the mammalian QSOX crystal structures show for the first time, to our knowledge, the plasticity and sophistication of the Cys-Gly-His-Cys motif, present in numerous redox-active proteins of the PDI family[18].

The expansion of multi-domain protein architectures contributes to the growth of the protein universe[19] and the development of complex species[20]. Rarely is it possible, however, to determine quantitatively how domain fusion contributes to protein function. Owing to its modular structure, QSOX provides an opportunity to quantify the benefit of concatenation of functional units. We measured the extent of this benefit by adding increasing concentrations of HsQSOX1(PDI) to catalytic amounts of HsQSOX1(Erv) to determine the ratio necessary to achieve the reaction rate of intact HsQSOX1 (Fig. 3d). We observed that the effective concentration of the disulphide-transferring module is increased by more than 2,500-fold by its concatenation to the disulphide-generating module through a poorly conserved linker (Supplementary Fig. 12). Our results emphasize the principle, applicable to design and *in vitro* evolution of new catalytic or signalling relays, that the function of proteins acting in tandem may be greatly improved by concatenation using flexible generic linkers.

Although mammalian cells are replete with PDI-family proteins[18], which contain diverse numbers and arrangements of redox-active and -inactive domains, QSOX is the only enzyme with an oxidoreductase domain homologous to PDI fused to a domain that generates disulphide bonds *de novo*. QSOX is also exceptional in having a primary localization outside of the endoplasmic reticulum. The QSOX structures reported here show how the two functions of the enzyme, generation of disulphides and transfer to substrate proteins, are permitted through a loose tethering of the two modules (Fig. 3e). On one hand, the fusion is sufficient to greatly increase the effective concentration of the two active sites, but on the other it allows an enormous range of motion. Understanding how this flexibility may further contribute to interactions with substrate must await identification of the native targets of QSOX catalysis in the late secretory pathway and extracellular environment.

METHODS SUMMARY

Protein preparation. TbQSOX and its mutants were produced as described[13]. Enzymes were purified using nickel-nitrilotriacetic acid (Ni-NTA), digested with thrombin and reapplied to Ni-NTA. Unbound material was collected, concentrated and purified by gel filtration. HsQSOX1(PDI) and MmQSOX1 (Cys76Ala/Cys455Ser) were produced in BL21(DE3) pLysS *E. coli* and purified as for TbQSOX. For crystallization, HsQSOX1(PDI) was treated with a dimethylamine–borane complex[21]. TbQSOX (Cys72Ser/Cys353Ser) and MmQSOX1 (Cys76Ala/Cys455Ser) were incubated before gel filtration with maleimide-functionalized polyethylene glycol (PEG) to separate $TbQSOX_C$ and $MmQSOX1_C$ from thiol-containing species.

Protein crystallization. TbQSOX crystals were grown by vapour diffusion over a well solution containing 14–18% (w/v) 2 kDa PEG monomethyl ether and 10% ethylene glycol. Crystals of $TbQSOX_C$ were grown over 20% (w/v) 3.35 kDa PEG, 0.2 M sodium sulphate and 0.5% (w/v) polyvinylpyrrolidone K15. Crystals of methylated HsQSOX1(PDI) were grown over 20% (w/v) 3.35 kDa PEG and 0.2 M lithium sulphate monohydrate. Crystals of $MmQSOX1_C$ were grown over 0.1 M MES buffer, pH 6.5, and 12% (w/v) 20 kDa PEG (orthorhombic) or 0.1 M HEPES buffer, pH 7.0, 10% (v/v) 1,5-pentanediol and 5% (v/v) glycerol (monoclinic).

Structure solution. The TbQSOX structure was determined by molecular replacement using a partial human QSOX structure (Protein Data Bank (PDB) code 3LLK) and a TbQSOX Trx1 homology model. The $TbQSOX_C$ structure was determined by molecular replacement using wild-type TbQSOX fragments. The HsQSOX1(PDI) structure was determined as described[22] (search models, PDB codes 3ED3 and 2E0Q). The $MmQSOX1_C$ structure was determined by molecular replacement using HsQSOX1(PDI) and HsQSOX1(Erv).

FRET spectroscopy. Pacific Blue C_5-maleimide labelling was according to manufacturer's instructions. The excitation wavelength was 400 nm, and energy transfer was measured with reference to enzyme containing $FADH_2$. TbQSOX (Ser160Cys) wavelength scans in the presence of dithiothreitol (1 mM) were initiated within 10 s after mixing and completed within 1 min. TbQSOX (Ser160Cys) kinetic experiments were conducted using a stopped-flow fluorimeter with a 420 nm long-pass emission filter.

Full Methods and any associated references are available in the online version of the paper.

Received 2 August 2011; accepted 28 May 2012.
Published online 15 July 2012.

1. Riemer, J., Bulleid, N. & Herrmann, J. M. Disulfide formation in the ER and mitochondria: two solutions to a common process. *Science* **324,** 1284–1287 (2009).
2. Tu, B. P. & Weissman, J. S. Oxidative protein folding in eukaryotes: mechanisms and consequences. *J. Cell Biol.* **164,** 341–346 (2004).
3. Kodali, V. K. & Thorpe, C. Oxidative protein folding and the quiescin–sulfhydryl oxidase family of flavoproteins. *Antioxid. Redox Signal.* **13,** 1217–1230 (2010).
4. Antwi, K. *et al.* Analysis of the plasma peptidome from pancreas cancer patients connects a peptide in plasma to overexpression of the parent protein in tumors. *J. Proteome Res.* **8,** 4722–4731 (2009).
5. Song, H. *et al.* Loss of *Nkx3.1* leads to the activation of discrete downstream target genes during prostate tumorigenesis. *Oncogene* **28,** 3307–3319 (2009).
6. Schulman, S., Wang, B., Li, W. & Rapoport, T. A. Vitamin K epoxide reductase prefers ER membrane-anchored thioredoxin-like redox partners. *Proc. Natl Acad. Sci. USA* **107,** 15027–15032 (2010).
7. Goodstadt, L. & Ponting, C. P. Vitamin K epoxide redutase: homology, active site and catalytic mechanism. *Trends Biochem. Sci.* **29,** 289–292 (2004).
8. Zanata, S. M. *et al.* High levels of active quiescin Q6 sulfhydryl oxidase (QSOX) are selectively present in fetal serum. *Redox Rep.* **10,** 319–323 (2005).
9. Ostrowski, M. C. & Kistler, W. S. Properties of a flavoprotein sulfhydryl oxidase from rat seminal vesicle secretion. *Biochemistry* **19,** 2639–2645 (1980).
10. Jaje, J. *et al.* A flavin-dependent sulfhydryl oxidase in bovine milk. *Biochemistry* **46,** 13031–13040 (2007).
11. Raje, S. & Thorpe, C. Inter-domain redox communication in flavoenzymes of the quiescin/sulfhydryl oxidase family: role of a thioredoxin domain in disulfide bond formation. *Biochemistry* **42,** 4560–4568 (2003).
12. Heckler, E. J., Alon, A., Fass, D. & Thorpe, C. Human quiescin-sulfhydryl oxidase, QSOX1: probing internal redox steps by mutagenesis. *Biochemistry* **47,** 4955–4963 (2008).
13. Kodali, V. K. & Thorpe, C. Quiescin sulfhydryl oxidase from *Trypanosoma brucei*: catalytic activity and mechanism of a QSOX family member with a single thioredoxin domain. *Biochemistry* **49,** 2075–2085 (2010).
14. Mitra, P. & Pal, D. New measures for estimating surface complementarity and packing at protein–protein interfaces. *FEBS Lett.* **584,** 1163–1168 (2010).
15. Inaba, K., Takahashi, Y. H., Ito, K. & Hayashi, S. Critical role of a thiolate-quinone charge transfer complex and its adduct form in *de novo* disulfide bond generation by DsbB. *Proc. Natl Acad. Sci. USA* **103,** 287–292 (2006).
16. Fass, D. The Erv family of sulfhydryl oxidases. *Biochim. Biophys. Acta* **1783,** 557–566 (2008).

17. Alon, A., Heckler, E. J., Thorpe, C. & Fass, D. QSOX contains a pseudo-dimer of functional and degenerate sulfhydryl oxidase domains. *FEBS Lett.* **584,** 1521–1525 (2010).
18. Appenzeller-Herzog, C. & Ellgaard, L. The human PDI family: versatility packed into a single fold. *Biochim. Biophys. Acta* **1783,** 535–548 (2008).
19. Levitt, M. Nature of the protein universe. *Proc. Natl Acad. Sci. USA* **106,** 11079–11084 (2009).
20. Tordai, H., Nagy, A., Farkas, K., Bányai, L. & Patthy, L. Modules, multidomain proteins and organismic complexity. *FEBS J.* **272,** 5064–5078 (2005).
21. Walter, T. S. *et al.* Lysine methylation as a routine rescue strategy for protein crystallization. *Structure* **14,** 1617–1622 (2006).
22. DiMaio, F. *et al.* Improved molecular replacement by density- and energy-guided protein structure optimization. *Nature* **473,** 540–543 (2011).

Supplementary Information is linked to the online version of the paper at www.nature.com/nature.

Acknowledgements S. Rogotner and O. Dym helped in growing the $TbQSOX_C$ crystals. We thank T. Ilani and A. Horovitz for reading of the manuscript and N. Nelson and his research group for help with X-ray data collection. A. Moseri assisted with high-performance liquid chromatography. This study was funded by the Israel Science Foundation. D.F. and A.A. acknowledge the Kimmelman Center for Macromolecular Assemblies for additional support. C.T. and V.K.K. acknowledge National Institutes of Health (NIH) grant GM26643. The molecular movie was produced using the University of California San Francisco Chimera package from the Resource for Biocomputing, Visualization and Informatics (supported by NIH grant P41 RR001081).

Author Contributions A.A. designed experiments, expressed, purified and crystallized proteins, and, together with D.F., solved and refined the TbQSOX, $TbQSOX_C$ and $MmQSOX1_C$ structures. A.A. also performed the FRET and crosslinking experiments. I.G. improved the TbQSOX crystals. Y.G. grew the $MmQSOX1_C$ crystals. V.K.K. and C.T. provided plasmids and helped to design and analyse experiments. F.D. and D.B. accomplished the molecular replacements to solve the HsQSOX1(PDI) structure. T.M. performed the mass spectrometry experiments and analyses. G.H. helped to design and analyse the FRET experiments and assisted with operation of the fluorimeter. D.F. expressed proteins, performed oxygen consumption measurements and designed and analysed the experiments. A.A. and D.F. wrote the manuscript.

Author Information Atomic coordinates and structure factors for the TbQSOX, $TbQSOX_C$ and HsQSOX1(PDI) structures have been deposited with the Protein Data Bank under accession codes 3QCP, 3QD9 and 3Q6O, respectively. The $MmQSOX1_C$ coordinates and structure factors have been deposited with accession codes 3T58 (orthorhombic) and 3T59 (monoclinic). Reprints and permissions information is available at www.nature.com/reprints. The authors declare no competing financial interests. Readers are welcome to comment on the online version of this article at www.nature.com/nature. Correspondence and requests for materials should be addressed to D.F. (deborah.fass@weizmann.ac.il).

METHODS

Plasmid construction. TbQSOX mutants not previously available were made using the QuikChange mutagenesis kit (Stratagene) on the basis of the published TbQSOX expression plasmid[13]. HsQSOX1(PDI) spans residues 33–272 of HsQSOX1. The coding sequence for this region was cloned between the NdeI and BamHI sites of the pET-15b vector (Novagen). The HsQSOX1 protein used for activity assays spans residues 33–546 of HsQSOX1. The coding sequence for this region was cloned between the NdeI and BamHI sites of the pET-15b vector. The thrombin cleavage site and His_6 tag encoded by the vector were excised by NcoI and NdeI restriction and replaced with a His_6 tag only. The MmQSOX1 (Cys76Ala/Cys455Ser) double mutant was made by mutation of a *Mus musculus* synthetic QSOX1 gene codon optimized for protein production in *E. coli* (GenScript). The coding sequence for residues 36–550 was inserted into pET-15b between the NdeI and BamHI sites.

Protein preparation. TbQSOX and its mutants were produced in the Origami 2 (DE3) *E. coli* cell strain as described[13], except that bacteria were grown in Luria–Bertani media. The MmQSOX1 (Cys76Ala/Cys455Ser) double mutant was produced in the BL21 (DE3) pLysS *E. coli* strain. Cells were lysed by sonication in 20 mM sodium phosphate buffer, pH 7.4, 500 mM NaCl and 20 mM imidazole, supplemented with protease inhibitors (100 $\mu g\,ml^{-1}$ phenylmethylsulphonyl fluoride (PMSF) and 1 $\mu g\,ml^{-1}$ of leupeptin, aprotinin and pepstatin A). Crude extract was clarified by centrifugation at 40,000*g* for 1 h. The enzymes, containing N-terminal His_6 tags, were purified from the soluble fraction by nickel-nitrilotriacetic acid (Ni-NTA) chromatography (GE Healthcare). Eluted TbQSOX, TbQSOX mutants and the MmQSOX1 mutant were exchanged into 20 mM sodium phosphate buffer, pH 7.4, 100 mM NaCl and 20 mM imidazole using a PD-10 desalting column (GE Healthcare). Thrombin (10 U per mg protein) was added, and the cleavage reaction was incubated for 2 h at 25 °C. PMSF was added to a concentration of 1 mM to inhibit thrombin and the protein was reapplied to Ni-NTA resin. Unbound material was collected, concentrated and applied to a PD-10 desalting column pre-equilibrated with crystallization stock buffer (10 mM Tris, pH 8, and 100 mM NaCl) and then applied to a HiLoad 16/60 Superdex 75 gel filtration column (GE Healthcare) under the same buffer conditions. Alternatively, size-exclusion chromatography was performed in 20 mM sodium phosphate buffer, pH 7.5, and 200 mM NaCl. The TbQSOX (Cys72Ser/Cys353Ser) mutant was incubated before gel filtration with maleimide-functionalized 5 kDa polyethylene glycol (PEG). The MmQSOX1 (Cys76Ala/Cys455Ser) mutant was incubated with maleimide-functionalized 10 kDa PEG. The fraction lacking the Cys 69–Cys 350 disulphide bond (for TbQSOX) or the Cys 73–Cys 452 disulphide bond (for MmQSOX1) became doubly modified by PEG, which increased its hydrodynamic radius sufficiently to allow separation from $TbQSOX_C$ or $MmQSOX1_C$ (Supplementary Fig. 4). Owing to high yields of the MmQSOX1 mutant, the peak corresponding to the protein not modified by PEG was collected, reconcentrated and loaded again on the gel-filtration column to achieve complete separation from PEG-modified material.

HsQSOX1, HsQSOX1(PDI) and HsQSOX1(Erv) were produced in the BL21(DE3) pLysS *E. coli* strain and purified as for wild-type TbQSOX, except that the HsQSOX1 construct lacked a thrombin cleavage site and was therefore subjected to gel filtration after the first Ni-NTA column without the cleavage step. Before crystallization, HsQSOX1(PDI) was treated with a dimethylamine–borane complex to methylate lysines as described[21], and the protein was then separated from excess reagents by gel filtration in crystallization stock buffer.

Protein crystallization. Crystals were grown by hanging-drop vapour diffusion at 293K. Wild-type TbQSOX and TbQSOX (Ser160Cys) crystals were grown over a well solution containing 14–18% (w/v) 2 kDa PEG monomethyl ether (MME) and 10% (v/v) ethylene glycol. Crystals were transferred to a solution containing 20% (w/v) 2 kDa PEG MME and 20% (v/v) ethylene glycol, and then transferred to a 1:1 mixture of mineral oil and Paratone oil (Exxon) before flash freezing. Crystals of $TbQSOX_C$ were grown over a well solution containing 20% (w/v) 3.35 kDa PEG, 0.2 M sodium sulphate and 0.5% (w/v) polyvinylpyrrolidone K15. Crystals were transferred to a solution of 25% (v/v) glycerol, 0.2 M sodium sulphate and 20% (w/v) 3.35 kDa PEG and flash frozen. Crystals of the methylated HsQSOX1(PDI) were grown over a well solution containing 20% (w/v) 3.35 kDa PEG and 0.2 M lithium sulphate monohydrate. Crystals were transferred to a solution of 25% (v/v) glycerol, 20% (w/v) 3.35 kDa PEG and 0.2 M lithium sulphate monohydrate and flash frozen. Crystals of $MmQSOX1_C$ grown over a well solution containing 0.1 M MES buffer, pH 6.5, 12% (w/v) 20 kDa PEG were of the orthorhombic space group $P2_12_12_1$. These crystals were transferred to a solution of 0.1 M MES, pH 6.5, 12% (w/v) 20 kDa PEG and 25% (v/v) glycerol for freezing. Crystals of $MmQSOX1_C$ grown over a well solution containing 0.1 M HEPES buffer, pH 7.0, 10% (v/v) 1,5-pentanediol and 5% (v/v) glycerol were of the monoclinic space group $P2_1$. These crystals were transferred to a solution of 0.1 M HEPES, pH 7.0, 10% (v/v) 1,5-pentanediol and 25% (v/v) glycerol, and then transferred to a 1:1 mixture of mineral oil and Paratone oil for freezing.

Data collection. Diffraction data were collected at 100K. Data for wild-type TbQSOX crystals, HsQSOX1(PDI) and the monoclinic ($P2_1$) $MmQSOX1_C$ crystals were collected at a wavelength of 1.544 Å on a RU-H3R generator (Rigaku) equipped with a RaxisIV++ image plate system and Osmic mirrors. TbQSOX data were collected to 2.3 Å resolution from crystals of space group $P2_12_12$. Data for the HsQSOX1(PDI) were collected to 2.05 Å resolution from a crystal of space group $P2_12_12_1$. Data for monoclinic $MmQSOX1_C$ were collected to 2.8 Å resolution from a crystal of space group $P2_1$. Data from the $TbQSOX_C$ crystals, of space group $P2_1$, were collected to 3.3 Å resolution at a wavelength of 0.9769 Å on European Synchrotron Radiation Facility (ESRF) beamline ID23-1 using a helical data-collection strategy (for rod-shaped crystals). Data for orthorhombic ($P2_12_12_1$) $MmQSOX1_C$ were collected to 2.4 Å resolution at a wavelength of 1.000 Å on ESRF beamline ID29. Data for TbQSOX (Ser160Cys) crystals were collected to 2.6 Å resolution at a wavelength of 1.005 Å on ESRF beamline BM30. Data from TbQSOX, TbQSOX (Ser160Cys), $MmQSOX1_C$ monoclinic and $MmQSOX1_C$ orthorhombic crystals were processed and scaled using DENZO and SCALEPACK[23]. $TbQSOX_C$ and HsQSOX1(PDI) data were processed and scaled using iMOSFLM[24] and SCALA[25].

Structure solution. The wild-type TbQSOX structure was determined by molecular replacement using Phaser[26]. The helical core of the partial human QSOX structure (Protein Data Bank (PDB) code 3LLK) and a homology model of the TbQSOX Trx1 domain generated using Modeller[27] were used as search models. The $TbQSOX_C$ structure was determined by molecular replacement using fragments of the wild-type TbQSOX structure as search models in Phaser. The HsQSOX1(PDI) structure was determined by molecular replacement, using search models from yeast Mpd1 (PDB code 3ED3) and K53E thioredoxin from *Sulfolobus tokodaii* (PDB code 2E0Q). A template based on 3ED3, trimmed of non-conserved loops and side chains, was first placed using Phaser; gaps in the template were rebuilt and refined using density- and energy-guided optimization with Rosetta[22]. This allowed placement of the second domain by Phaser using a trimmed model based on 2E0Q, which underwent the same rebuilding procedure. Model refinement was performed using CNS[28] or Phenix[29] incorporating the TLSMD[30] procedure. In all cases, model rebuilding was done using Coot[31]. The $MmQSOX1_C$ structure was determined using the $P2_12_12_1$ data and the structures of HsQSOX1(PDI) and HsQSOX1(Erv) as search models in Phaser. Chain A of the refined $MmQSOX1_C$ model was positioned (four copies) in the $P2_1$ $MmQSOX1_C$ crystal unit cell using Phaser and further refined using CNS[28]. As assessed using MolProbity[32], there are no Ramachandran outliers in the structures reported herein.

Surface complementarity. Normalized interface packing (NIP) and normalized surface complementarity (NSc) were calculated according to ref. 33. The interface area between the Trx1 domain and the ψErv/Erv domains in $TbQSOX_C$ was calculated to be 867 $Å^2$. The NIP and NSc values were calculated to be 2.33×10^{-4} and 3.87×10^{-4}, respectively. The interface area between the comparable domains of $MmQSOX1_C$ was calculated to be 892 $Å^2$. The NIP and NSc values were calculated to be 2.49×10^{-4} and 3.70×10^{-4}, respectively. The QSOX NIP values are greater than ~75% of the NIP values for evolved complexes and less than ~85% of the NIP values for crystal contacts of monomeric proteins. The QSOX NSc values are greater than ~80% of the NSc values for evolved complexes and less than 83% of the NSc values for crystal contacts. By comparison, the interface area of the two subunits in the Erv2 dimer (PDB code 1JR8) was calculated to be 1233 $Å^2$ and the NIP and NSc values were 1.81×10^{-4} and 2.30×10^{-4}, respectively. The Erv2 NIP value is greater than 39% of the NIP values for evolved complexes (that is, squarely within the expected packing values for complexes) and less than 95% of the NIP values for crystal contacts (that is, the packing is much better than most crystal contacts). The Erv2 NSc value is greater than 57% of the NSc values for evolved complexes (that is, the surface complementarity is typical of evolved complexes) and less than ~94% of the NSc values for crystal contacts (that is, the complementarity is much better than for most crystal contacts).

FRET spectroscopy. All mutants used in the FRET studies were purified as for the wild-type enzymes, except that a five- to tenfold molar excess of C_5 Pacific Blue-maleimide (Invitrogen) was added after gel filtration. A second gel filtration was then performed to remove excess dye. The fraction corresponding to the peak of the gel filtration chromatogram was used for further study. FRET experiments were performed in a 1 cm pathlength cuvette at a protein concentration of 6.3 nM in 20 mM sodium phosphate buffer, pH 7.5, 200 mM NaCl and 0.5 mM EDTA. Excitation was at a wavelength of 400 nm. As the fluorescence acceptor, namely the bound FAD cofactor, is an intrinsic part of QSOX enzymes, quantum yield of fluorophore conjugated at various positions in the native protein in the absence of acceptor could not be directly determined. Instead, acceptor absorbance was diminished *in situ* by reduction to $FADH_2$, which results in an 83% decrease in

absorbance at 454 nm. Reduction was accomplished by the addition of glucose oxidase and glucose to deplete the dissolved oxygen and DTT to reduce the TbQSOX active site as described in Supplementary Fig. 3. Donor fluorescence was monitored kinetically until an abrupt increase was observed, indicating conversion to $FADH_2$. Reduced state wavelength scans were then collected. Distances were calculated as described in Supplementary Table 2.

Mass spectrometry. Gel fragments were treated with varying protease combinations at 37 °C in 50 mM ammonium bicarbonate. Peptide mixtures were extracted from the gels with 80% acetonitrile and 1% trifluoroacetic acid (TFA), and the organic solvent was evaporated in a vacuum centrifuge. The resulting peptide mixtures were reconstituted in 80% formic acid and immediately diluted 1:10 with Milli-Q water before analysis. Liquid chromatography–tandem mass spectrometry (LC–MS/MS) was performed using a 15 cm reversed-phase spraying fused-silica capillary column (inner diameter, 75 μm) made in-house and packed with 3 μm ReproSil-Pur C_{18}AQ media (Dr. Maisch GmbH) using an UltiMate 3000 Capillary/Nano LC System (LC Packings, Dionex). The LC system was used in conjunction with an LTQ Orbitrap (Thermo Fisher Scientific) operated in the positive ion mode and equipped with a nanoelectrospray ion source. Peptides were separated with a 50-min gradient from 5 to 65% acetonitrile (buffer A, 5% acetonitrile, 0.1% formic acid and 0.005% TFA; buffer B, 90% acetonitrile, 0.2% formic acid and 0.005% TFA). The voltage applied to the union to produce an electrospray was 1.2 kV. The mass spectrometer was operated in the data-dependent mode. Survey mass spectrometry scans were acquired in the Orbitrap with the resolution set to a value of 60,000. Up to the six most intense ions per scan were fragmented and analysed in the linear trap. For the analysis of peptides, survey scans were recorded in the Fourier transform mode followed by data-dependent collision-induced dissociation of the six most intense ions in the linear ion trap. Raw data files were searched with MASCOT (Matrix Science) against a Swissprot database modified by inclusion of the relevant mutants. The program MassMatrix[34] was used for identification of disulphide bonds and BS3 crosslinks from MGF files.

QSOX enzyme assays. Sulphydryl oxidase activity was measured at 25 °C by monitoring oxygen consumption in a Clarke-type oxygen electrode (Hansatech Instruments Ltd). Buffer conditions were 50 mM potassium phosphate buffer, pH 7.5, 300 mM NaCl and 1 mM EDTA. HsQSOX1(PDI) and HsQSOX1(Erv) were mixed in the oxygen electrode chamber and reactions were initiated by injection of DTT to a concentration of 1 mM. For comparison, *E. coli* thioredoxin was prepared as described[35] and used in place of HsQSOX1(PDI). Intact HsQSOX1 activity was re-measured[12] for reference by diluting the enzyme to 100 nM into the oxygen electrode chamber and initiating the reaction by injection of DTT to 1 mM. Turnover numbers were calculated per FAD cofactor. Oxygen consumption by HsQSOX1(Erv) alone is indistinguishable from background rates under these conditions (not shown). Oxygen consumption in the presence of varying concentrations of HsQSOX1(PDI) alone or thioredoxin alone was minimal.

23. Otwinowski, Z. & Minor, W. Processing of X-ray diffraction data collected in oscillation mode. *Methods Enzymol.* **276,** 307–326 (1997).
24. Leslie, A. G. W. Recent changes to the MOSFLM package for processing film and image plate data. *Joint CCP4 + ESF-EAMCB Newslett. Protein Crystallogr.* **no. 26** (1992).
25. Evans, P. Scaling and assessment of data quality. *Acta Crystallogr. D* **62,** 72–82 (2006).
26. McCoy, A. J. *et al. Phaser* crystallographic software. *J. Appl. Cryst.* **40,** 658–674 (2007).
27. Eswar, N., Eramian, D., Webb, B., Shen, M. Y. & Sali, A. Protein structure modeling with MODELLER. *Methods Mol. Biol.* **426,** 145–159 (2008).
28. Brünger, A. T. *et al.* Crystallography & NMR system: a new software suite for macromolecular structure determination. *Acta Crystallogr. D* **54,** 905–921 (1998).
29. Afonine, P. V., Grosse-Kunstleve, R. W. & Adams, P. D. The Phenix refinement framework. *CCP4 Newslett.* **no. 42** (2005).
30. Painter, J. & Merritt, E. A. Optimal description of a protein structure in terms of multiple groups undergoing TLS motion. *Acta Crystallogr. D* **62,** 439–450 (2006).
31. Emsley, P. & Cowtan, K. *Coot*: model-building tools for molecular graphics. *Acta Crystallogr. D* **60,** 2126–2132 (2004).
32. Chen, V. B. *et al.* MolProbity: all-atom structure validation for macromolecular crystallography. *Acta Crystallogr. D* **66,** 12–21 (2010).
33. Mitra, P. & Pal, D. New measures for estimating surface complementarity and packing and protein–protein interfaces. *FEBS Lett.* **584,** 1163–1168 (2010).
34. Xu, H., Zhang, L. & Freitas, M. A. Identification and characterization of disulfide bonds in proteins and peptides from tandem MS data by use of the MassMatrix MS/MS search engine. *J. Proteome Res.* **7,** 138–144 (2008).
35. Gross, E. *et al.* Generating disulfides enzymatically: reaction products and electron acceptors of the endoplasmic reticulum thiol oxidase Ero1p. *Proc. Natl Acad. Sci. USA* **103,** 299–304 (2006).